FIRST RESULTS FROM THE SOHO ULTRAVIOLET CORONAGRAPH SPECTROMETER

J. L. KOHL[1], G. NOCI[2], E. ANTONUCCI[3], G. TONDELLO[4], M. C. E. HUBER[5], L. D. GARDNER[1], P. NICOLOSI[4], L. STRACHAN[1], S. FINESCHI[1], J. C. RAYMOND[1], M. ROMOLI[2], D. SPADARO[6], A. PANASYUK[1], O. H. W. SIEGMUND[7], C. BENNA[9], A. CIARAVELLA[5,*], S. R. CRANMER[1], S. GIORDANO[9], M. KAROVSKA[1], R. MARTIN[10], J. MICHELS[1], A. MODIGLIANI[2], G. NALETTO[4], C. PERNECHELE[4], G. POLETTO[8] and P. L. SMITH[1]

[1]*Harvard-Smithsonian Center for Astrophysics, Cambridge, MA 02138, U.S.A.*
[2]*Università di Firenze, I-50125 Firenze, Italy*
[3]*Osservatorio Astronomico di Torino, I-10025 Pino Torinese, Italy*
[4]*Università di Padova, I-35131 Padova, Italy*
[5]*Space Science Dept., ESA/ESTEC, NL-2200 AG, Noordwijk, The Netherlands*
[6]*Osservatorio Astrofisico di Catania, I-95125 Catania, Italy*
[7]*Space Sciences Laboratory, University of California, Berkeley, CA 94720, U.S.A.*
[8]*Osservatorio Astrofisico di Arcetri, I-50125 Firenze, Italy*
[9]*Università di Torino, I-10125 Torino, Italy*
[10]*Institut d'Astrophysique Spatiale, F-91405 Orsay, France*

(Received 14 March 1997; accepted 18 June 1997)

Abstract. The SOHO Ultraviolet Coronagraph Spectrometer (UVCS/SOHO) is being used to observe the extended solar corona from 1.25 to 10 $R_\odot$ from Sun center. Initial observations of polar coronal holes and equatorial streamers are described. The observations include measurements of spectral line profiles for H I Lα and Lβ, O VI 1032 Å and 1037 Å, Mg X 625 Å, Fe XII 1242 Å and several others. Intensities for Mg X 610 Å, Si XII 499 Å, and 520 Å, S X 1196 Å, and 22 others have been observed. Preliminary results for derived H^0, O^{5+}, Mg^{9+}, and Fe^{11+} velocity distributions and initial indications of outflow velocities for O^{5+} are described. In streamers, the H^0 velocity distribution along the line of sight (specified by the value at e^{-1}, along the line of sight) decreases from a maximum value of about 180 km s^{-1} at 2 $R_\odot$ to about 140 km s^{-1} at 8 $R_\odot$. The value for O^{5+} increases with height reaching a value of 150 km s^{-1} at 4.7 $R_\odot$. In polar coronal holes, the O^{5+} velocity at e^{-1} is about equal to that of H^0 at 1.7 $R_\odot$ and significantly larger at 2.1 $R_\odot$. The O^{5+} in both streamers and coronal holes were found to have anisotropic velocity distributions with the smaller values in the radial direction.

1. Introduction

The Ultraviolet Coronagraph Spectrometer on the Solar and Heliospheric Observatory (UVCS/SOHO) is being used for spectroscopic observations of the extended solar corona. The instrument is designed to obtain the data for diagnostic techniques aimed at determining empirical values for densities, velocity distributions, and outflow velocities of hydrogen, electrons, and several minor ions.

The velocity distribution of neutral hydrogen in the corona tends to reflect the proton distribution as well, because the characteristic lifetime for a hydrogen atom at coronal densities is significantly shorter than typical coronal expansion times

[*]Also Osservatorio Astronomico di Palermo. Palermo, Italy.

Solar Physics **175:** 613–644, 1997.

(Withbroe *et al.*, 1982). For example, at $r = 2.5\ R_\odot$ in a low-density coronal hole, a newly created H I atom will move about 0.02 $R_\odot$, before it is ionized. The correspondence between neutral hydrogen velocities and protons has been discussed by Leer (1988), Olsen and Leer (1996), and Allen, Habbal, and Hu (1996).

This paper describes examples of UVCS/SOHO observations during the first year of operations, and the derivation of particle velocity distributions and outflow velocities in the extended corona. The results are derived from direct application of spectroscopic diagnostic techniques. For example, velocity distributions are derived directly from the observed line profiles. In the future, more accurate values are expected to be obtained through the development of self-consistent empirical models of the observed coronal structures. The accuracy and confidence in the values presented here are discussed in the text.

The primary goals of the UVCS/SOHO observations are to provide detailed empirical descriptions of the extended solar corona, and to use the descriptions to gain information about the physical processes controlling the large-scale and small-scale features of the extended corona and the acceleration and composition of the solar wind near the Sun.

Although it is premature at this stage to claim any definitive information in that regard, the observations have revealed several unexpected results. The most surprising are the velocity distributions in polar coronal holes for particles of different mass. The velocities deviate significantly from those of a thermal distribution. The O^{5+} line-of-sight (LOS) velocities above 2.1 $R_\odot$ are larger than those of a thermal distribution at 1×10^8 K and the O^{5+} velocities are much larger than the H^0 velocities. This difference in the velocity distributions of H^0 and O^{5+} suggest that a large fraction of the O^{5+} velocity distribution is not caused by transverse wave motions. There is also evidence that the O^{5+} velocity distribution in the solar radial direction is much narrower than in the LOS direction. These two results suggest that a significant fraction of the O^{5+} velocity distribution may be caused by ion cyclotron resonant acceleration of O^{5+} ions by high-frequency MHD waves (McKenzie, Banaszkiewicz, and Axford, 1995). However, there is no independent confirmation of the existence of such waves although several plausible processes for producing them have been proposed. It is not clear from the data if any of the proton velocity distribution along the LOS is caused by ion cyclotron resonance. However, the H^0 velocities along the LOS are larger than would be expected for a thermal distribution at the expected electron temperature (Ko *et al.*, 1997). The values for the proton velocities at e^{-1} ($v_{1/e}$) approach those predicted by McKenzie, Banaszkiewicz, and Axford (1995) for their ion-cyclotron resonance model.

Outflow velocities for O^{5+} reach values of 130 to 230 km s^{-1} in coronal holes within heliocentric distances of 3.0 $R_\odot$. Clear evidence for acceleration in the extended corona is observed. The particles do not appear to enter the extended corona at supersonic velocities. This information further constrains theoretical models aimed at identifying the dominant heating and acceleration processes.

UVCS/SOHO measurements of LOS velocity distributions near the base of equatorial streamers are much closer to those expected in a thermal distribution at the expected electron temperature, but there is a tendency for the more massive particles to have excess velocities. This behavior is more pronounced in regions of lower density. Future work should investigate the possibility that ion-cyclotron resonance is important in equatorial streamers as well as in coronal holes. The proton and O^{5+} outflow velocities in equatorial streamers appear to reach a value between 175 and 205 km s^{-1} near heliocentric heights of 7 $R_{\odot}$.

The UVCS results are not limited to the information presented here. A determination of chemical abundances in streamers indicates significant departures from photospheric values (Raymond *et al.*, 1997). There have been at least two spectroscopic observations of CMEs, one on 7 June 1996 and one on 23 December 1996. The latter observation indicates intensity increases by a factor of 500 in the H I Lyman lines and the presence of ions at low stages of ionization such as C III. Large spectral line shifts indicate particle flow velocities above 100 km s^{-1} along the LOS. There have also been observations of Comet SOHO 6 and 8 in H I Lα, observations of several stars at wavelengths shortward of the Hubble Space Telescope range that have not been seen since the Copernicus Mission, and observations of H I Lα in the ram direction of the solar system moving through the local interstellar cloud and of H I Lα and He I 584 Å in the wake direction.

2. The UVCS Instrument

The UVCS/SOHO has been described previously by Kohl *et al.* (1995) and, therefore, only a brief descripton is provided here. UVCS consists of a telescope spectrometer unit (TSU) and a remote electronics unit (REU). The TSU is a triple telescope with external and internal occultation and a high-resolution spectrometer assembly. Three spherical telescope mirrors focus co-registered images of the extended corona onto the three entrance slits of the spectrometer assembly. The spectrometer assembly consists of three channels:

– The Lα channel is a toric grating spectrometer that is optimized for line profile measurements of H I 1216 Å and may also be used for other spectral lines in the 1145 Å to 1287 Å spectral range. An extended wavelength range (1100 Å to 1361 Å) may be observed by rotating the grating.

– The O VI channel is a toric grating spectrometer that is optimized for measurements of the O VI lines at 1032 Å and 1037 Å and may also be used for other spectral lines in the 984 Å to 1080 Å (first-order) and 492 Å to 540 Å (second-order) spectral range. An extended wavelength range in first and second order (937 Å to 1126 Å and 469 Å to 563 Å, respectively) may be observed by rotating the grating. The O VI channel includes a convex mirror between the grating and the O VI detector to focus the H I 1216 Å (first-order) and Mg X 610 Å and 625 Å (second-order) radiations onto the O VI detector.

– The white-light channel (WLC) is a visible light polarimeter that measures polarized radiance in the 4500–6000 Å wavelength band.

The field of view (FOV) of UVCS is provided in Kohl *et al.* (1995). The instantaneous FOV is the portion of the solar image that passes through the entrance slits of the ultraviolet channels. The slit heights correspond to 40 arc min in the direction parallel to the limb tangent. The WLC has a 14 arc sec $\times$ 14 arc sec spatial field at the center of the UV instantaneous FOV. Internal mirror motions are used to step the instantaneous FOV from 1.2 to 10 $R_\odot$. Offset pointing adjustments with the UVCS pointing mechanism can be used to extend the FOV down to the solar limb and onto the disk or up to 12 $R_\odot$. UVCS can rotate its FOV about Sun-center in order to observe the full corona.

3. Diagnostic Techniques for the Extended Corona

Several diagnostic techniques were used to provide the information contained in this paper. The basic techniques have been described previously (Kohl and Withbroe, 1982; Withbroe *et al.*, 1982, 1985; Noci, Kohl, and Withbroe, 1987; van de Hulst, 1950), and therefore will be discussed only briefly here.

Hydrogen and ion velocity distributions are determined from measured spectral line profiles of H I Lα, O VI 1032 Å and other spectral lines. The shape of the profile depends on the velocity distribution of the particles emitting or scattering the detected photons. In general, spectral lines of the extended solar corona are formed by both collisional excitation followed by spontaneous radiative decay and by resonant scattering of light from deeper in the solar atmosphere. In the case of resonant scattering, the line shape is affected by the line profile of the incident light for non-90° scattering. However, the line shape is dominated by Doppler shifts that can be the result of several different types of particle motions (e.g., microscopic motions such as thermal motions or ion/cyclotron resonance induced motions, transverse wave motions, and macroscopic motions such as bulk outflow along a LOS through an extended object). The profiles can also be affected by variations in conditions along the LOS. There may be local sites with different densities and/or different local velocity distributions (e.g., foreground and background structures). There may be local non-Maxwellian velocity distributions. The LOS may pass through several flux tubes (i.e., regions of dissimilar magnetic field, electron temperature, bulk outflow, and MHD waves).

Contributions along the LOS can be affected by the angular dependence of resonant scattering. UVCS provides synoptic observations that can be used in the future to help determine the contributions to the profiles from structures along the LOS.

For near 90-deg scattering, which tends to be the case for observations above the limb, the angular dependence of resonant scattering and the line profile of the incident light have only a small effect on the observed profiles. Equations

describing the angular dependence of resonant scattering are provided in Withbroe *et al.* (1982). A model code, which utilizes those equations, was used to simulate observable spectral lines. It was found that for objects located in the plane of the sky or objects distributed along the LOS as if they are spherically symmetric, and for precisions of $\pm 10\%$, the observed line profile can be converted to a velocity distribution using the usual formula

$$\frac{\Delta\lambda}{\lambda_0} = \frac{V}{c} \,, \tag{1}$$

where $\Delta\lambda$ is the wavelength relative to the line center, λ_0, and c is the speed of light. This is the case for polar coronal holes and the equatorial streamers near solar minimum that are described in this paper.

Outflow velocities are determined by the Doppler dimming method. There are several ways of determining outflow velocities from Doppler dimming. Spectral lines of different ions can have different sensitivities to outflow velocity because of their different spectral line widths. The relevant line width is that determined by the velocity distribution in the direction of the incoming light to the corona. The curves in Figure 1 are for line widths corresponding to Maxwellian distributions at three different temperatures.

A detailed analysis requires an empirical model which uses as inputs, measured electron temperatures and electron densities. This information is used in the model to calculate the ionization balance terms R and predict the observed EUV intensity as a function of the outflow velocity. The model must also include the details of the resonant scattering process and any collisionally excited contribution to the spectral line.

In this paper, Doppler dimming and brightening of O VI lines are presented. The Doppler dimming of the O VI line at 1037.613 Å is particularly useful because pumping by C II 1037.018 Å extends its velocity sensitive range to include values from about 90 km s^{-1} to about 300 km s^{-1} (Noci, Kohl, and Withbroe, 1987). Pumping by C II occurs when the O^{5+} outflow velocity is large enough to shift the spectral line profile of the chromospheric C II light onto the coronal O VI scattering profile in the reference frame of the outflowing O^{5+}. Figure 1 shows the effect.

Because Doppler dimming only affects the resonantly scattered component of spectral lines and O VI lines have both resonantly scattered and collisionally excited contributions to the observed intensities, it is necessary to account for both contributions in deriving outflow velocities.

Noci, Kohl, and Withbroe (1987) describe a method whereby, the intensity ratio of the O VI 1032 Å and 1037 Å lines can be used to determine the outflow velocity. Their method can be understood in the following way. In the absence of resonant scattering, the line ratio is 2:1 because of the factor of 2 difference in the collision strengths. This is observed to be the case, for example, in the transition region. The ratio for resonant scattering is 4:1; a factor of two for the strength of the absorption and another factor of two because of the difference in the

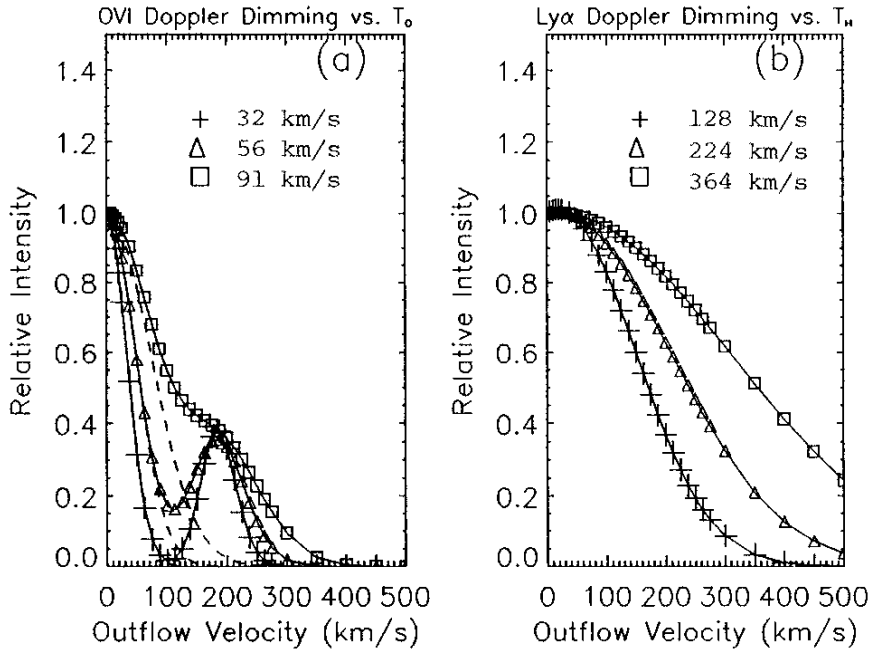

Figure 1. Doppler dimming curves for the resonantly scattered components of O VI 1032 Å and 1037 Å (a) and H I 1216 Å (b). In the plot on the left (a), the O VI 1037 curves are shown as solid lines and points. The curves for O VI 1032 Å follow those for O VI 1037 Å at the smallest velocities and then follow the dashed curves. The intensities are normalized to the value for zero outflow velocity. Curves are provided for three different values of $v_{1/e}$, in the direction of the incoming radiation to the corona from lower in the solar atmosphere. The curves include pumping of the coronal O VI 1037.613 Å line by chromospheric C II 1037.018 Å. The curves are for a single point in the plane of the sky.

intensity of the incident light from the transition region. Kohl and Withbroe (1982) have shown that, in the absence of C II 1037.018 Å pumping of the O VI 1037.613 line, the ratio determines the relative contributions of collisional excitation and resonant scattering to the observed intensity. It can be seen from Figure 1 that for radial velocity distributions with $v_{1/e}$ less than 56 km s^{-1}, resonant scattering of O VI 1032 Å becomes very small when the outflow velocity increases above about 125 km s^{-1} and the transition region O VI 1032 Å radiation is shifted off the coronal absorption profile. In that case, the line ratio would become 2 since the observed light would be only collisionally excited. However, if the outflow increases above 125 km s^{-1}, the C II line will begin to pump the O VI 1037 line and the ratio will drop below 2. The ratio would continue to decrease until the velocity reaches about 180 km s^{-1} when the C II line is centered on the O VI 1037 line. As the C II light is shifted further to the red, the resonantly scattered contribution begins to decrease and the line ratio approaches 2 at approximately 300 km s^{-1}.

The ratio is affected by the change in electron density with height in the corona since the collisional component scales as the square and the resonantly scattered component linearly. The ratio is affected by the velocity distribution in the direction of the incoming radiation to be scattered in the corona (see Figure 1). A detailed model is needed to derive precise values for the outflow velocities, but the general behavior of the outflow with height can be seen from the measured ratio.

4. Preliminary Identification of Spectral Lines Observed by UVCS/SOHO

The spectral lines detectable with UVCS/SOHO depend strongly on the observed coronal structure and the heliographic height. The strongest lines such as H I 1215.67 Å and 1025.72 Å, O VI 1031.96 Å and 1037.61 Å, and Mg X 609.76 Å and 624.95 Å are observed in polar coronal holes. Tables I and II list observed wavelengths and preliminary identifications for spectral lines observed in active region streamers on the east limb of the Sun on 23 and 24 July 1996 at about 1.5 $R_{\odot}$. A preliminary wavelength scale was used for the measured values. Identifications with low confidence are indicated by a question mark. Forbidden lines are indicated with double brackets and intercombination lines with closing brackets. Several spectral features that are present in the observations but currently unassigned, are not included in the tables. The intensity scale is in arbitrary units. The intensity values are approximately proportional to the observed values of integrated spectral radiance after background subtraction. Table I lists spectral lines detected with the UVCS/SOHO O VI detector. Lines with first order wavelengths longward of 1180 Å were observed via the path in the UVCS/SOHO O VI channel that includes an auxiliary convex mirror. Table II lists spectral lines detected with the UVCS/SOHO Lα Channel. Only first-order lines are detectable in the latter channel because of a magnesium floride window.

5. UVCS/SOHO Measurements of Coronal Spectral Line Profiles

UVCS has observed spectral line profiles of H I 1216 Å and 1026 Å, O VI 1032 Å and 1037 Å, Fe XII 1242 Å, S X 1196 Å, and several other lines in streamers, and of H I 1216 Å, O VI 1032 Å, and 1037 Å and Mg X 625 Å in polar coronal holes. The observed spectral line profiles are discussed in Sections 6 and 7.

The profiles have been corrected for an instrument characteristic that effecively smears the wavelengths such that a broad line wing with an amplitude of about 1 –3% of the line peak is produced. The zero integral functions are used to correct this effect by redistributing the photons in the artificial line wing. The zero integral functions were derived from observations of the narrow interplanetary H I Lα line. The functions for the Lα channel and the O VI channel are similar, but not identical. Convolution of the zero integral function with the observed line profile yields a

Table I
Preliminary identifications for observed spectral lines in the O VI channel

Wavelength[a] 1st order	Wavelength[a] 2nd order	Int.[b]	λ_{ID}	Identification
949.97		7.1	950.15	H I Lδ, [Si IX] $2p2\ ^3P_1 - 2p2\ ^1S_0$
972.56		7.0	972.54	H I Lγ
974.06	487.03	9.3	487.04	[Fe XIII] $3s^2 3p^2\ ^3P_2 - 3s3p^3\ ^5S_1$
981.10	490.55	9.7	490.20	[Ar XIII] $2p^2\ ^3P_2 - 2s2p^3\ ^5S_2$
982.60	491.30	9.0	491.44	[S XIII] $2s^2\ ^1S_0 - 2s2p\ ^3P_1$
993.26	496.21	13.8	496.25	[Ar XIV] $2s^2 2p\ ^2P_{3/2} - 2s2p^2\ ^4P_{1/2}$
998.77	499.39	485	499.37	Si XII $2s\ ^2S_{1/2} - 2p\ ^2P_{3/2}$
1018.88		1.3	1018.60	[Ar XII] $2p^3\ ^4S_{3/2} - 2p^3\ ^2D_{5/2}$
1020.04	510.02	11.1	510.08	[Fe XIII] $3s^2 3p^2\ ^3P_2 - 3s3p^3\ ^5S_2$
1025.73		50.1	1025.72	H I Lβ
1028.10		1.8	1028.04	[Fe X] $3d\ ^4D_{7/2} - 3d\ ^4F_{7/2}$
1031.96		819	1031.91	O VI $2s\ ^2S_{1/2} - 2p\ ^2P_{3/2}$
1037.50		286	1037.61	O VI $2s\ ^2S_{1/2} - 2p\ ^2P_{1/2}$
1041.26	520.63	242	520.66	Si XII $2s\ ^2S_{1/2} - 2p\ ^2P_{1/2}$
1054.87		1.5	1054.90	[Ar XII] $2p^3\ ^4S_{3/2} - 2p^3\ ^2D_{3/2}$
1070.63	535.32	10.4	535.32	[S XII] $2s^2 2p\ ^2P_{3/2} - 2s2p^2\ ^4P_{3/2}$
1100.14	550.07	50.0	550.01	Al XI $2s\ ^2S_{1/2} - 2p\ ^2P_{3/2}$
1115.52	557.76	21.8	557.74	Ca X $3s\ ^2S_{1/2} - 3p\ ^2P_{3/2}$
1196.19		24.2	1196.25	[S X] $2p^3\ ^4S_{3/2} - 2p^3\ ^2D_{5/2}$
1215.67		18100	1215.67	H I Lα
1219.71	609.86	1530	609.76	Mg X $2s\ ^2S_{1/2} - 2p\ ^2P_{3/2}$
1238.57		13.0	1238.82	N V $2s\ ^2S_{1/2} - 2p\ ^2P_{3/2}$
1241.80		47.5	1242.03	[Fe XII] $3p^3\ ^4S_{3/2} - 3p^3\ ^2P_{3/2}$
1249.90	624.95	520	624.95	Mg X $2s\ ^2S_{1/2} - 2p\ ^2P_{1/2}$
1260.42	629.73	226	629.73	O V $2s^2\ ^1S_0 - 2s2p\ ^1P_1$

[a] In Å.
[b] In arbitrary units.

correction that, when subtracted from the observed profile, provides an improved approximation of the coronal profile. After about three iterations, convergence is obtained.

The results of this corrective procedure were checked by comparing the corrected line profile of chromospheric H I Lα with observations from other instruments (Gouttebroze *et al.*, 1978; Wilhelm, 1996) and by comparing UVCS/SOHO observations of H I Lα in streamers with typical streamer profiles observed with UVCS/Spartan 201 (see Strachan *et al.*, 1994). An example of an uncorrected line profile together with the same profile after correction is provided in Figure 2.

Table II
Preliminary identifications for observed spectral lines in the Lα channel

Wavelength[a]	λ_{ID}	Int.[b]	Identification
1196.25	1196.25	28.1	[S X] $2p^3\,{}^4S_{3/2} - 2p^3\,{}^2D_{5/2}$
1215.67	1215.67	18680	H I Lα
1238.56	1238.82	12.9	N V $2s\,{}^2s_{1/2} - 2p\,{}^2P_{3/2}$
1241.69	1242.03	60.1	[Fe XII] $3p^3\,{}^4S_{3/2} - 3p^3\,{}^2p_{3/2}$
1277.17	1277.23	2.3	[Ni XIII] $3p^3\,{}^3P_1 - {}^1S_0$
1349.89	1349.38	28.8	[Fe XII] $3p^3\,{}^4S_{3/2} - 3p^3\,{}^2P_{1/2}$

[a] In Å.
[b] In arbitrary units.

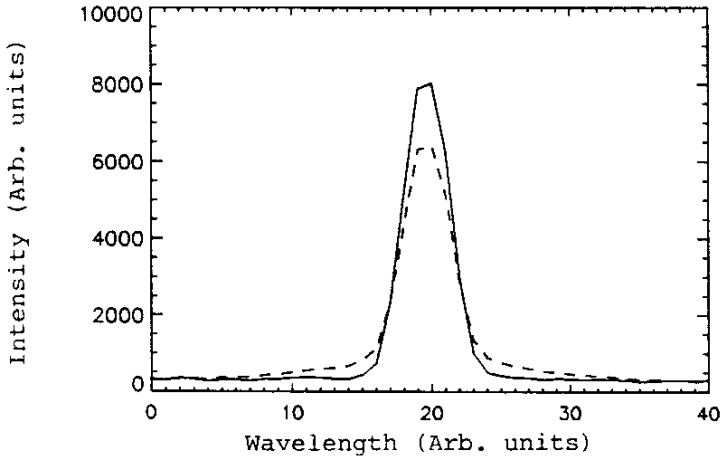

Figure 2. Example of profiles corrected (solid) and uncorrected (dashed) for an instrument effect that removes photons from the profile core and creates an artificial line wing.

The corrected profiles are normally curve-fit with a standard algorithm that minimizes the following equation for χ^2:

$$\chi^2 \equiv \sum_{i=1}^{N} \left(\frac{y_i - y(x_i; a_1 \ldots a_M)}{\sigma_i} \right)^2 , \tag{2}$$

where σ_i are the standard deviations for each data point (x_i, y_i), N is the number of data points used for the fit and M is the number of free parameters. The standard deviations are assumed to equal $n^{1/2}$ where n is the number of counts for each data point. The resulting minimum value of χ^2 is used to estimate the goodness-of-fit. It is customary to use the reduced χ^2 for this purpose which is the minimum χ^2 divided by the degrees of freedom $\nu = N - M$. Tables providing the probability of exceeding $\nu^{-1}\chi^2_{\rm min}$ in are provided in Bevington (1969). For the case of the spectral

line profile curve-fits discussed in this paper which typically have about 18 deg of freedom. A $\nu^{-1}\chi^2_{\rm min}$ value of about 1.4 corresponds to a probability for exceeding that value of 10%. This value has been adopted in this paper as an indicator of an acceptable curve-fit. Larger values for $\nu^{-1}\chi^2_{\rm min}$ might be caused by small deviations from the ideal expression due, for example, to the angular dependence of resonant scattering (Withbroe *et al.*, 1982), and by departures from the assumed distribution of standard deviations or by instrument effects. Several such cases are discussed in Sections 6 and 7.

In addition to the above instrument characteristics, the observed spectral lines are broadened by the usual optical point spread function of the spectrometer. Laboratory measurements of the effective instrument profile were performed at both the complete instrument level and for the spectrometer alone. The results are described in Kohl *et al.* (1995), Pernechele *et al.* (1995), and Gardner *et al.* (1996). In-flight measurements have confirmed the laboratory results for the Lα channel and refined the value of the laboratory upper limit for the O VI channel. Since the UVCS/SOHO telescope is highly vignetted and the exposed telescope area depends on the heliographic height of the observation, the spectral resolution can be a function of the observed height. This effect has been determined to be rather small and is ignored in this paper. The spectral resolution also depends on the slit width used for each observation and the quantization error of the detector. The FWHM of the instrument function for each observation is provided along with the other descriptions of the observations in Sections 6 and 7.

The observed line profiles can have contributions from instrument stray light plus F corona and, in the case of H I Lα, interplanetary hydrogen. These contributions are negligible in streamers at most of the heliocentric heights discussed here, but can be significant in coronal holes. In Section 7, constrained curve fits are described for removing these backgrounds.

6. Measurements of Velocity Distributions for H^0, O^{5+}, and Fe^{11+} in Streamers

Figures 3–5 provide several examples of spectral line profiles from an equatorial region of the extended solar corona observed on 12 October 1996 where the wavelength scale is converted to LOS velocity using Equation (1). This structure appears to be a helmet streamer in H I Lα and H I Lβ, but it has a bifurcated appearance in the O VI and Fe XII lines (see Figure 6).

In general, there are four quantities that could affect the H I Lα and O VI 1032 Å intensities in the streamer. They are the electron temperature, the electron density, the elemental abundance, and Doppler dimming. Detailed modeling is expected to help identify the quantities and processes responsible for the observed intensities of Figure 6 (Noci *et al.*, 1997; Raymond *et al.*, 1997).

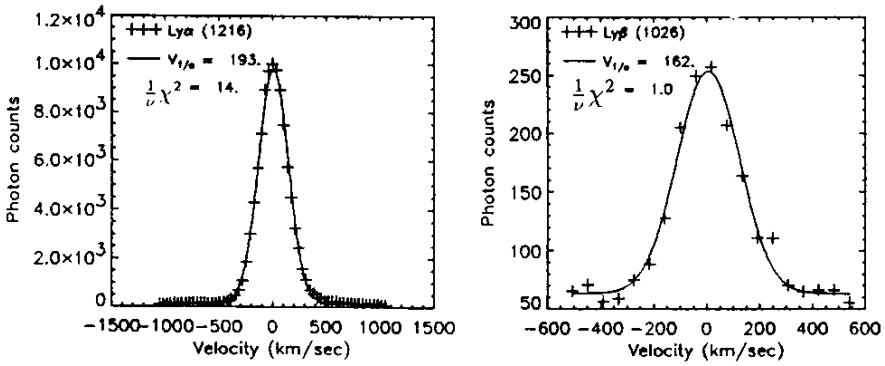

Figure 3. UVCS 12 October 1996 observations of H I Lα and Lβ profiles for an equatorial streamer above the west limb (position angle = 270°) centered at a heliocentnc height of 2.1 $R_\odot$. The spatial resolution elements for Lα and Lβ are 0.23 × 8.4 arc min and 0.23 × 21 arc min, the FWHM of the instrument line profiles are 0.28 Å and 0.23 Å, respectively, and the integration time is 3600 s. Curve fits for a single Gaussian plus a constant background are shown. The data points are shown by crosses and the fitted curve by a solid line. The fully corrected best fit $v_{1/e}$, and the $\nu^{-1}\chi^2$ are provided in the figure.

The profiles have been corrected for the artificial line wing effect described in Section 5. Each of the corrected profiles are curve-fit to a single Gaussian plus a constant background. This provides a value for the velocity ($v_{1/e}$) corresponding to the Doppler half width, which is corrected for the finite instrumental resolution and provided in each figure. The FWHM of the instrumental profiles for the instrument configuration used for the observation are also provided. Several types of motions which may contribute to the measured velocity distribution are listed in Section 3.

The H I Lα and Lβ profiles at a projected heliographic height of 2.1 $R_\odot$ are provided in Figure 3. The H I Lα profile is for the upper bright region of the streamer as seen in Figure 6. Profiles for other regions are similar. To improve statistics, Lβ is for a slice across the entire streamer. In the case of H I Lβ, the value of $\nu^{-1}\chi^2 = 1.0$ indicates a good fit within the limitations of the rather low statistical precision of the data. In the case of Lα, which has much higher statistical precision, $\nu^{-1}\chi^2 = 14$.

Figure 7 provides values for the elements of $\nu^{-1}\chi^2$ for the Lα profile. It can be seen that the largest contributions come from near the base of the profile. The fit to the center portion of the profile is very good and indicates high confidence in the derived $v_{1/e}$.

The most likely candidates for explaining the poorer fit at the base are the following: (1) departures from a Maxwellian velocity distribution along the LOS, (2) a region along the LOS with a broader velocity distribution than that of the dominant contribution from the streamer, and (3) a small inaccuracy in the function used to remove the artificial line wings induced by the instrument or some other instrument effect. Less likely explanations include foreground and background

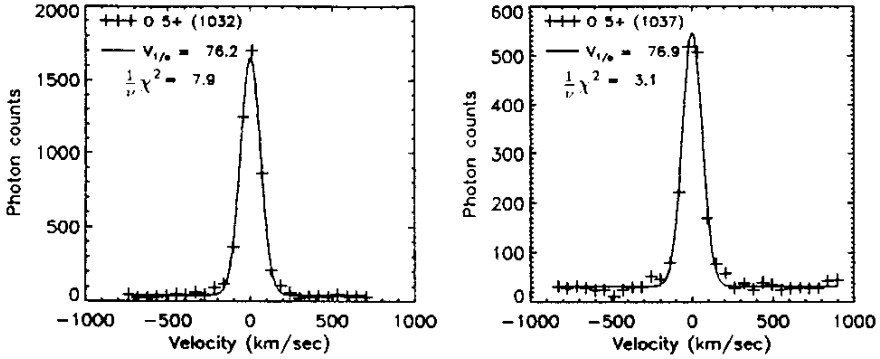

Figure 4. UVCS 12 October 1996 observations of O VI 1032 Å and 1037 Å profiles for an equatorial streamer above the west limb (position angle $= 270^{\circ}$) centered at a heliocentric height of 2.1 $R_{\odot}$. The spatial elements for both lines are 0.23×9.3 arc min, the FWHM of the instrument line profiles are 0.23 Å and the exposure time is 3600 s. Curve fits for a single Gaussian plus a constant are shown. The data points are shown by crosses and the fitted curve by a solid line. The fully corrected best fit $v_{1/e}$ and the $\nu^{-1}\chi^2$ are provided in the figure.

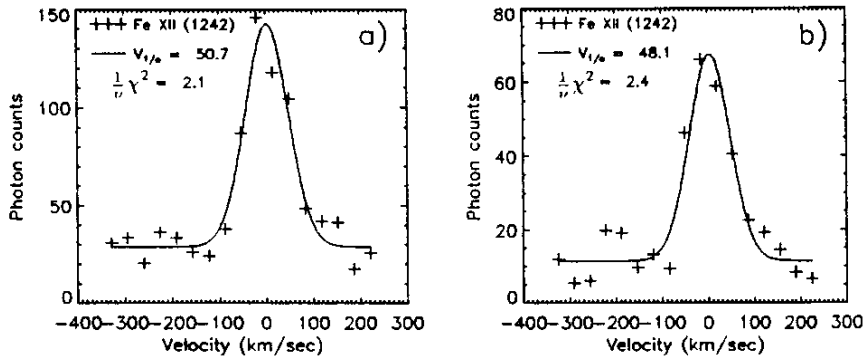

Figure 5. UVCS 12 October 1996 observations of Fe XII 1242 Å for an equatorial streamer above the west limb (position angle $= 270^{\circ}$) centered at a heliocentric height of 2.1 $R_{\odot}$. The spatial resolution element across the entire streamer (a) is 21 arc min, and the spatial element across the upper bright region (b) is 8.4 arc= min. The FWHM of the instrumental profile is 0.18 Å, and the integration time is 3600 s. Curve fits for a single Gaussian plus a constant are shown. The data points are shown by crosses and the fitted curve by a solid line. The fully corrected best fit $v_{1/e}$ and the $\nu^{-1}\chi^2$ are provided in the figure.

structures with LOS outflows of about 240 km s^{-1}, but this requires extremely divergent magnetic field geometries or much larger outflow velocities than are indicated by the Doppler dimming results provided in Sections 8 and 9.

The difference in $\nu^{-1}\chi^2$ for the two lines is believed to result, primarily, from the larger values of σ_i for H I Lβ. Similar values for $\nu^{-1}\chi^2$ can be obtained for Lα if a subset of the data, corresponding to a much smaller exposure time, is used.

The velocity distributions derived from the two lines correspond to $v_{1/e}$ of 193 km s^{-1} and 162 km s^{-1}, respectively for Lα and Lβ.

The uncertainty is considerably smaller for Lα compared to Lβ because of the larger number of counts. There is a tendency for Lβ to be narrower than Lα in streamers (see Figure 8). The difference might have to do with line formation mechanisms. A significant fraction of Lβ is collisionally excited. That intensity is proportional to the square of the electron density (see discussion in Section 3). The smaller $v_{1/e}$ for Lβ might be explained by smaller $v_{1/e}$ in the most dense regions of streamers along the LOS.

O VI 1032 and 1037 profiles for the upper bright region in the streamer are provided in Figure 4. The statistical precision is at an intermediate level and the $\nu^{-1}\chi^2$ values indicate a departure from a single Gaussian at the precision level of the data. Values for the r.m.s. velocity (i.e., the second moment of the distribution) are equal to $2^{-1/2}$ of $v_{1/e}$ as expected for a Gaussian distribution. Hence, the O^{5+} LOS velocity distribution approximates a single Gaussian.

The velocity distributions derived from the two O VI lines are very similar. They correspond to $v_{1/e}$ of 76 km s^{-1} and 77 km s^{-1}, respectively, for the 1032 and 1037 lines. The two values are equal within the uncertainties.

The Fe XII 1242 Å profile for the upper bright region of the streamer is provided in Figure 5(b). An Fe XII profile with better statistics and integrated over the entire segment of the slit across the streamer is provided in Figure 5(a). The two profiles have equal widths to within the uncertainties. Some departures from a single Gaussian within the precision of the data is indicated by the values of $\nu^{-1}\chi^2$ although the relationship between $v_{1/e}$ and $v_{\text{r.m.s.}}$ indicates a Gaussian shape.

The best-fit values of $v_{1/e}$ for H I 1216 Å, O VI 1032 Å, S X 1196 Å, and Fe XII 1242 Å for several heliographic heights in the 12 October 1996 streamer are provided in Figure 8. The profiles used in Figure 8 are integrated over a slice of the corona that extends across the entire structure and is centered on the designated height (see Figure 6).

In the case of H I 1216 Å, it is found that $v_{1/e}$ reaches a maximum value of about 195 km s^{-1} at a heliographic height of 2.1 $R_\odot$ and falls to about 150 km s^{-1} at 5.0 $R_\odot$. The O VI values are smaller (about 70 km s^{-1} at 2.1 $R_\odot$) and increase with height to about 150 km s^{-1} at 5 $R_\odot$. The Fe XII values are about 50 km s^{-1} at 2.1 $R_\odot$. S X 1196 Å values are also shown. Figure 8 includes values of $v_{1/e}$ for H I Lα and O VI 1032 Å in an equatorial streamer observed on 5 February 1997. The profiles for the two observations are similar but not identical. The 5 February 1997 observations indicate that the H I Lα values of $v_{1/e}$ continue to decrease slowly for heights up to 8 $R_\odot$.

Although the velocity distributions of coronal particles of different mass observed by UVCS never correspond to those expected in a thermal distribution, the velocities at the base of streamers come the closest. If we define the kinetic temnerature as one that describes all of the observed particle motions, the velocities at 1.5 $R_\odot$

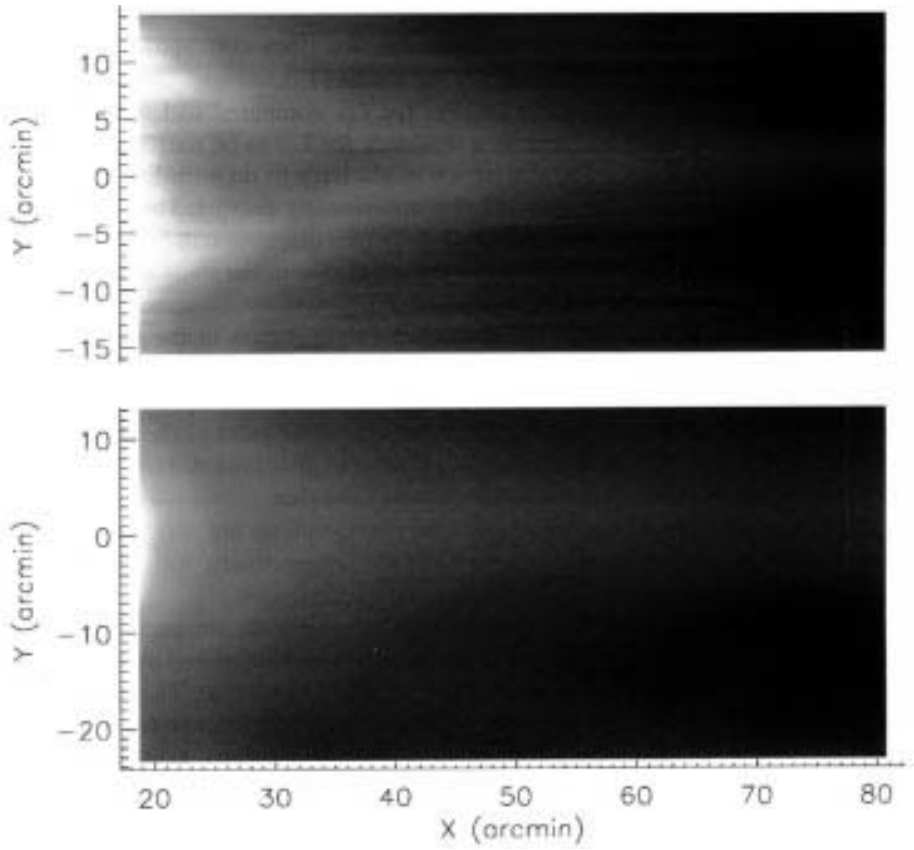

Figure 6. Images of the UVCS 12 October 1996 observation of an equatorial streamer above the west limb in H I Lα and O VI 1032 Å. The images result from an interpolation between strips of the corona corresponding to the UVCS entrance slit. The region has a strikingly different appearance in the two spectral lines. Fe XII images resemble those of O VI 1032 Å. The spatial scales are solar coordinates in arc min where the origin is at the center of the disk, the x axis is approximately in the heliographic west direction and the positive y axis is the projected heliographic north direction.

correspond to 2.0×10^6 K for H^0, 3.2×10^6 K for O^{5+} and 5.3×10^6 K for Fe^{11+}. The electron temperature derived from the charge state balance of hydrogen is 2.4×10^6 K (assuming the proton outflow velocity is less than 80 km s^{-1} and no Doppler dimming) which is similar to that derived from the Lα profile. At 2.4×10^6 K, O^{5+} would have $v_{1/e} = 50$ km s^{-1} which is within 10 km s^{-1} of the observed value. At the same temperature, Fe^{11+} would have 27 km s^{-1} which is within 13 km s^{-1} of the observed value. The kinetic temperatures corresponding to the observed values of $v_{1/e}$ at 3 $R_\odot$ have larger deviations from a thermal distribution.

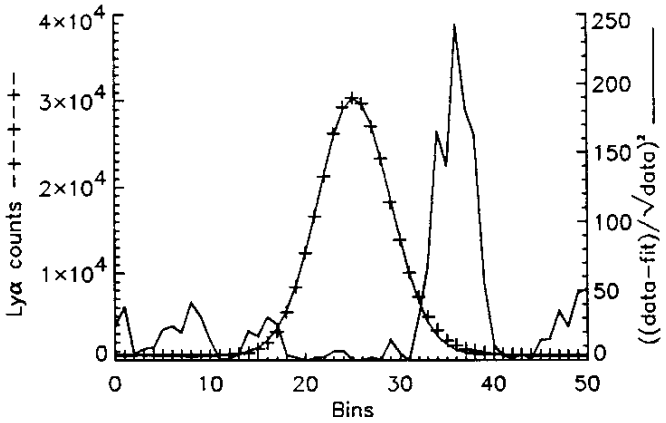

Figure 7. Chi-squared elements (solid line) and H I Lα spectral line profiles (solid line with crosses) for equatorial streamer of 12 October 1996 versus detector bins in the wavelength dispersion direction.

Figure 9 provides values of $v_{1/e}$ for O VI 1032 Å in three regions of the equatorial streamer. The region with the smallest O VI intensity also has smaller oxygen $v_{1/e}$ than the brighter regions.

Based on the values of polarized radiance from the WLC (see Section 8) and the intensity of Lα, it is believed that the streamer axis, which is dark in O VI, has a higher electron and proton density than the bright region.

It is interesting that the observed velocities come closest to a thermal distribution in the higher density regions (i.e., lower heights and streamer axis). In the lower density regions, the velocities of the more massive particles more strongly exceed those of a thermal equilibrium plasma at the observed hydrogen temperature. A plausible explanation for this behavior is that some process is preferentially accelerating particles of higher mass, and collisions are driving the velocities toward thermal equilibrium. The data suggest that such a process may be occurring throughout the streamer, but collisions are effectively thermalizing the plasma in the higher density regions. The velocity distributions in lower density coronal holes (see Section 7) may be providing even stronger evidence of such a process.

Values of reduced $\nu^{-1}\chi^2_{\rm min}$ for the equatorial streamer profiles are provided in each of the figures that show profiles. It can be seen that the values for H I Lα are rather large, while the curve-fits in Figure 3 appear to be reasonably good. The high statistical accuracy of the points causes $\nu^{-1}\chi^2_{\rm min}$ to be very sensitive to small differences between the observations and an ideal Gaussian curve. Data with poorer statistics such as the Fe XII 1242 Å line in Figure 5 may have similar departures from an ideal Gaussian, but the larger values of σ_i result in a much smaller value of $\nu^{-1}\chi^2_{\rm min}$.

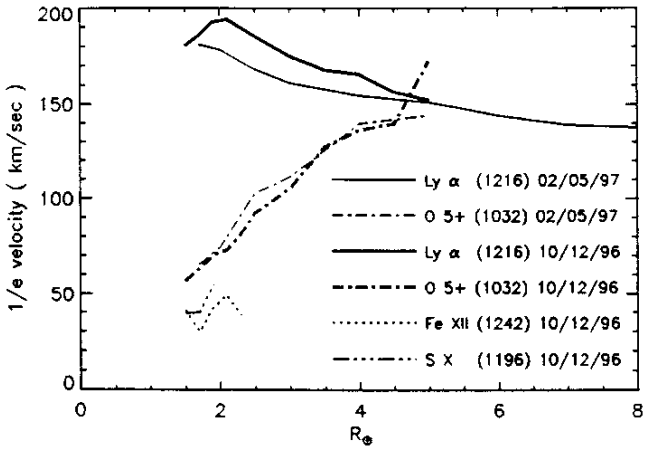

Figure 8. Plot of $v_{1/e}$ vs height for 12 October 1996 observation of a slice across the entire equatorial streamer. The profiles are dominated by the brightest regions. Values of $v_{1/e}$ are provided for H I Lα, O VI 1032 Å, S X 1196 Å, and Fe XII 1242 Å. Values for a similar streamer observed on 5 February 1997 are also provided.

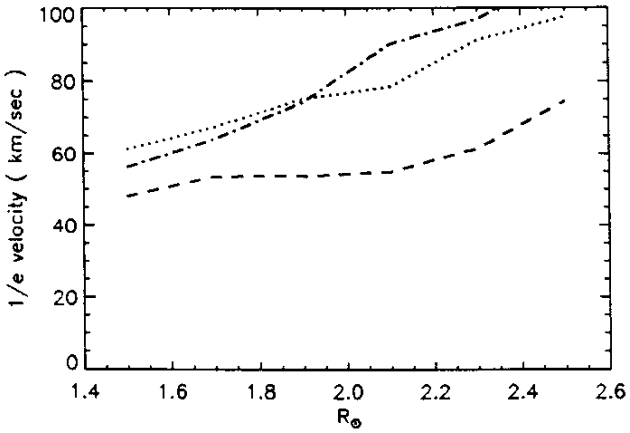

Figure 9. Velocity at e^{-1} of the peak of the LOS velocity distribution for O^{5+} versus heliocentric height for regions of the 12 October 1996 equatorial streamer. The curves for the two bright regions in O VI 1032 Å are shown as dots and as dot-dashes and the dark region curve is shown as dashes.

7. Measurements of Velocity Distributions for H^0, O^{5+}, and Mg^{9+} in Polar Coronal Holes

Figure 10 is an example of a H I Lα line profile in a polar coronal hole where the wavelength scale is converted to LOS velocity using Equation (1). The profile was measured at a central heliographic height of 3.0 $R_\odot$ on 11 May 1996 by the

UVCS/SOHO instrument. A curve-fit to a single Gaussian plus a constant is shown. The value of $\nu^{-1}\chi^2_{\rm min}$ is 7.6. The Gaussian that minimizes χ^2 clearly fails to fit the peak of the line and the base of the line. Such profiles are typical of those observed in polar coronal holes by UVCS/SOHO.

The integrated intensity of the observed line is 1.9×10^8 photons s^{-1} cm^{-2} sr^{-1}. The expected interplanetary intensity is about 3×10^7 photons s^{-1} cm^{-2} sr^{-1} and is broadened by the instrument profile FWHM $= 0.28$ Å. Laboratory measurements of instrumental stray light for observations at 2.7 $R_\odot$ determined that the equivalent stray light intensity for Lα is about 1×10^{-8} of the intensity of Lα at Sun center or about 4.5×10^7 photons s^{-1} cm^{-2} sr^{-1}. It has the profile of chromospheric H I Lα (Gouttebroze *et al.*, 1978) convolved with the instrument profile. In-flight determinations of a combination of stray light and the ultraviolet F corona based on detection of Si III 1206 and C III 977 (ions normally not expected in the corona) are consistent with laboratory values (Gardner *et al.*, 1996). A constrained curve fit was used to account for the stray light plus F corona and interplanetary Lα in the observation and to fit the coronal component to a Gaussian curve. For the curve fits, the line shapes of the stray light plus F corona and interplanetary Lα and the intensity of the stray light plus F corona were held fixed. All other quantities were allowed to vary. The result is shown in Figure 10(a). The coronal component is well fit to a single Gaussian curve with a velocity corresponding to the Doppler half width $v_{1/e} = 230$ km s^{-1}. Any other coronal contributions to the observed profile would be at the level of the uncertainties in the stray light plus F corona and interplanetary Lα intensities. A plasma in thermodynamic equilibrium with the expected electron temperature of coronal holes at this height (about 1×10^6 K) would have a hydrogen $v_{1/e}$ of 129 km s^{-1}.

These H I Lα profiles observed by UVCS/SOHO are reminiscent of H I Lα profiles observed in coronal holes in 1993 by the Ultraviolet Coronal Spectrometer on the Spartan 201 spacecraft (Kohl, Strachan, and Gardner, 1996). That paper described curve-fits of the profiles to two Gaussians, in the case of the south polar coronal hole, and attributed part of the more narrow component to the tip of an obvious streamer along the LOS. The remainder of the narrow component was attributed to either less obvious streamers or to sites along the LOS with smaller values of $v_{1/e}$. Another alternative explanation for the non-Gaussian shape is local non-Maxwellian velocity distributions along the LOS.

The derived coronal component at 3.0 $R_\odot$ from UVCS/SOHO has $v_{1/e} = 230$ km s^{-1}. This value is within 20% of the average broad component at 2.5 $R_\odot$ from Spartan 201 which has $v_{1/e} = 288$ km s^{-1}. The Spartan narrow components are a factor of 10 brighter than the expected stray light levels. UVCS/SOHO synoptic images clearly show that streamers are outside the LOS for polar coronal hole observations at 3.0 $R_\odot$ in the June 1996 time frame. This suggests that the broad components observed by SOHO are formed in the coronal holes.

Figures 11–13 provide several examples of spectral line profiles from the north polar coronal hole observed by UVCS/SOHO in June 1996. Figure 12 provides

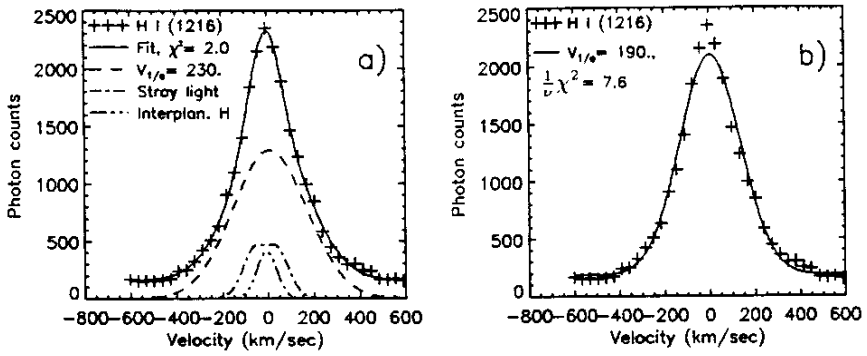

Figure 10. UVCS 11 May 1996 observations of H I Lα profiles for the south polar coronal hole (position angle $= 180^{\circ}$) centered at a heliocentric height of 3.0 $R_{\odot}$. The spatial resolution element is 0.23×38.5 arc min, the FWHM of the instrument line profile is 0.28 Å, and the integration time is 10 800 s. Computer fits for a single Gaussian plus a constant (b) and three Gaussians plus a constant (a) are shown. Constrained fits were used to account for interplanetary Lα and stray light plus F corona. The data points are shown as crosses, the coronal profile by dashes and the fitted profile by a solid line. The fully corrected best fit $v_{1/e}$ and the $\nu^{-1}\chi^2_{\rm min}$ are provided on the figure.

profiles of O VI 1032 Å and 1037 Å with the slit centered at 2.1 $R_{\odot}$. The low intensity of the O VI emission at that height accounts for the fairly small number of accumulated counts. The spatial element used for the integration includes both polar plumes and inter-plume regions.

The 1032 profile has a complex shape that appears to consist of one Gaussian, which accounts for most of the line intensity, plus a very narrow component. The width of the narrow component is indistinguishable from the instrument profile FWHM. The ratio of the 1032 narrow component intensity to the disk intensity corresponds to that expected from in-flight measurement of instrument stray light plus F corona. Hence, it is believed that the narrow spikes on the profiles at this height are due to stray light. Observations of a polar coronal hole on 7 April 1996 with about the same observational parameters, were similar.

Figure 12 shows curve-fits to the 1032 and 1037 lines. A background of about 200 counts has been subtracted from the data. The $\nu^{-1}\chi^2_{\rm min}$ of 2.7 is considered acceptable. The Doppler half widths of the broad components of the 1032 and 1037 profiles correspond to $v_{1/e}$ of about 485 km s^{-1}.

The variations of $v_{1/e}$ with heliocentric height for H I Lα, O VI 1032 Å, and 1037 Å are provided in Figure 14 for observations of the north polar coronal hole from 7 April 1996 and the June 1996 data. The $v_{1/e}$ for both the April and June 1996 observations at 2.1 $R_{\odot}$ are much larger than expected. For example, the $v_{1/e}$ of O^{5+} for a plasma in thermodynamic equilibrium at the expected electron temperature of about 1×10^6 K is 32 km s^{-1}.

There are several plausible explanations for the large LOS velocities. It is unlikely that outflow velocities make a large contribution. Expected outflow velo-

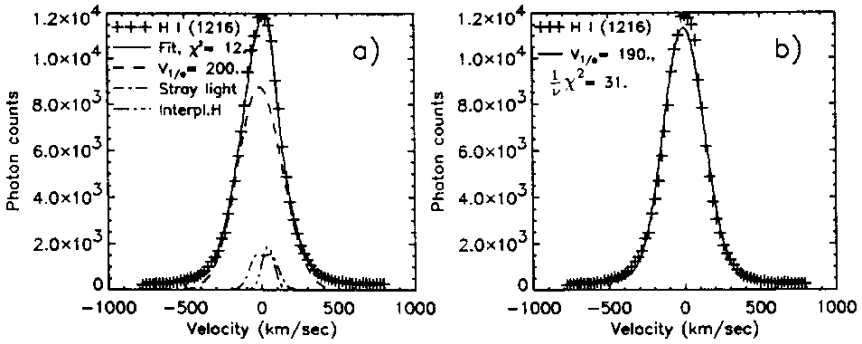

Figure 11. UVCS/SOHO 21 June 1996 observations of the H I Lα profile for the north polar coronal hole (position angle $= 0.0^{\circ}$) centered at a heliocentric height of 2.1 $R_{\odot}$. The spatial resolution element is 0.35×21.7 arc min, the FWHM of the instrument line profile is 0.23 Å and the integration time is 31 800 s. Computer fits to a single Gaussian plus a constant (b) and three Gaussians plus a constant (a) are shown. Constrained curve fits were used to account for interplanetary Lα and stray light plus the F corona. The data points are shown as crosses the coronal profile by dashes and the fitted profile by a solid line. The best fit $v_{1/e}$ and the $\nu^{-1}\chi^2_{\min}$ are provided in the figure.

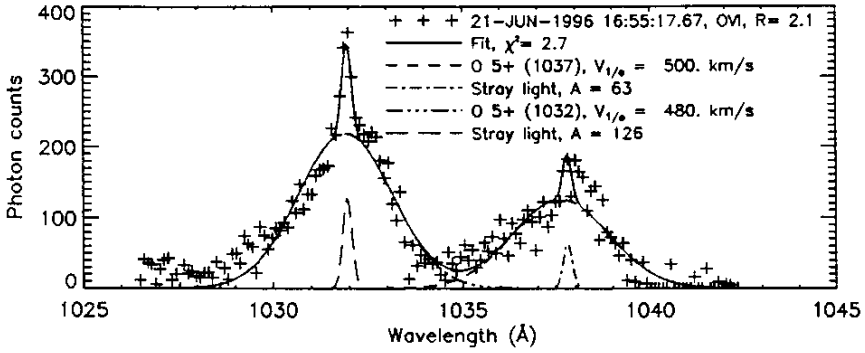

Figure 12. UVCS/SOHO 21 June 1996 observations of O VI 1032 Å and 1037 Å profiles for the north polar coronal hole (Position angle $= 0.0^{\circ}$) centered at a heliocentric height of 2.1 $R_{\odot}$. The spatial resolution element is 0.35×20.3 arc min, the FWHM of the instrument line profile is 0.25 Å, and the integration time is 31 800 s. Computer fits for two Gaussians plus a constant are shown for each of the two lines. Constrained curve fits were used to account for conbributions from stray light plus the F corona. The data points are shown as crosses, coronal profiles by dashes and the fitted profile by a solid line. The best fit $v_{1/e}$ and $\nu^{-1}\chi^2_{\min}$ are provided in the figure.

cities at 2.1 $R_{\odot}$ (see Strachan *et al.*, 1993) are about 150 km s^{-1} to 250 km s^{-1} and the component along the LOS would be significantly smaller and would not be expected to account for very much of the observed line width. If other macroscopic motions such as turbulence are responsible for the large $v_{1/e}$, they might be expected to affect H^0 as well, but the H^0 have smaller velocities than those of O^{5+} above 2 $R_{\odot}$ (see Figure 14).

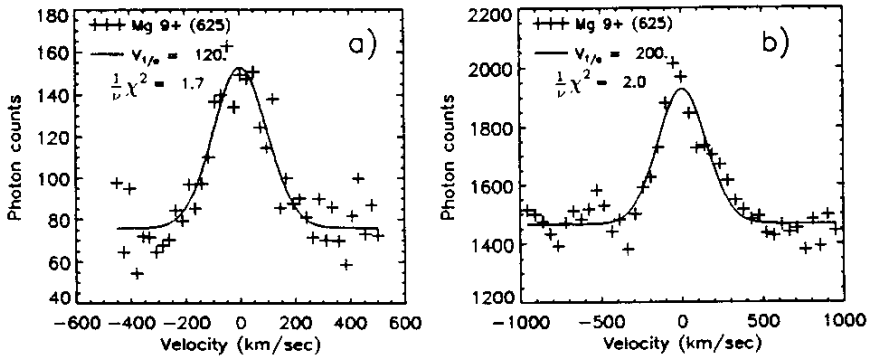

Figure 13. UVCS/SOHO observations of Mg X 625 Å for the north polar coronal hole (position angle $= 0.0^{\circ}$). An observation centered at 1.5 $R_{\odot}$ was made on 17 June 1996 (a) and one centered at 1.75 $R_{\odot}$ was made on 19 June 1996 (b). The spatial resolution elements are 0.70 × 7.35 arc min (a) and 0.70 × 21.7 arc min (b). The instrumental FWHM are 0.22 Å (a) and 0.23 Å (b). The data points are shown as crosses and the curve fit to a single Gaussian plus a constant is shown as a solid line. The best fit $v_{1/e}$ and the $\nu^{-1}\chi^2_{\rm min}$ are provided in the figure.

Microscopic velocities might be due, in part, to the remnant of the thermal distribution from lower heights and they might also be due, in part, to ion-cyclotron resonant acceleration by high-frequency MHD waves (McKenzie, Banaszkiewicz, and Axford, 1995). There might also be a contribution to the observed velocity distribution from transverse wave motions (Withbroe *et al.*, 1985).

Figure 11 provides a profile of H I Lα in the coronal region where the O VI profiles of Figure 12 were observed and during the same period of time. The profile has been curve-fit to a single Gaussian plus a constant background. The $\nu^{-1}\chi^2_{\rm min}$ value is 31, indicating a low confidence in the goodness-of-fit. The high precision data indicate a deviation from a single Gaussian near the base of the profile. The profile was also curve fit in the same manner described earlier for the 11 May 1996 observation (see Figure 10). The stray light plus F corona levels for observations at 2.1 $R_{\odot}$ are somewhat higher than for the observations at 3.0 $R_{\odot}$. The curve fit provides a reasonable fit to the constrained values for the stray light plus F corona, interplanetary Lα and a single Gaussian component for the coronal profile. The value of $\nu^{-1}\chi^2$ for this high precision data reflects rather small departures from the fitted curve that may be due to a variety of causes. The derived value for $v_{1/e} = 200$ km s^{-1}.

Figure 13 provides profiles of Mg X 625 Å observed on 17 and 19 June 1996 at heliocentric heights centered at 1.5 and 1.75 $R_{\odot}$, respectively, in the north coronal hole. Single Gaussian fits yielded $v_{1/e}$ of 130 and 210 km s^{-1}, respectively, for the two heights.

Polar plumes are apparent in both the O VI and H I intensities at 1.7 $R_{\odot}$ (see Figure 15). The plumes are brightest near the center of the slit projection, which has

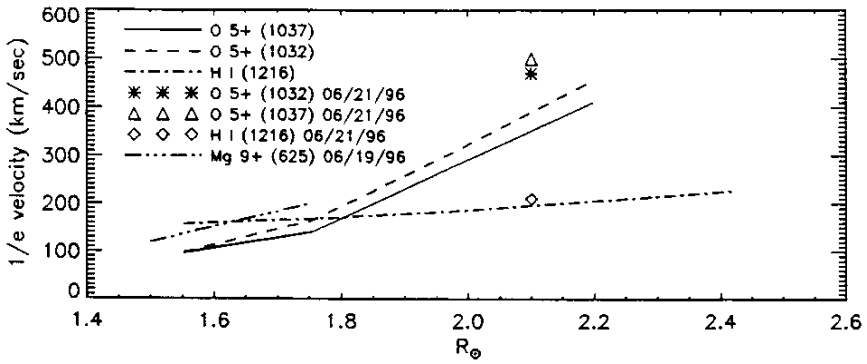

Figure 14. UVCS/SOHO measurements of $v_{1/e}$ versus heliocentric height for line-of-sight velocity distributions derived from H I Lα, O VI 1032 Å and 1037 Å and Mg X 625 Å for polar coronal holes observed on 7 April 1996 and June 1996. The values of $v_{1/e}$ are for single Gaussian fits to the line after removal of stray light, F corona and interplanetary H I Lα.

a higher latitude and a smaller heliocentric height than the regions corresponding to the extremities of the slit.

Figure 16 provides spectral line profiles for O VI 1032 in a region of the north polar coronal hole observed on 7 June 1996. Profiles are shown for a concentration of polar plumes at a heliocentric height of 1.7 $R_\odot$ and a region between two concentrations of plumes. The profiles were curve-fit to two Gaussians plus a constant background. The stray light plus F corona and interplanetary Lα are a very small contribution to the profile. Neither profile in Figure 16 can be well fit to a single Gaussian curve. The two Gaussian fits reveal that the narrow component is a much larger fraction of the total line intensity for the concentration of plumes than for the region between plume concentrations. The widths of the narrow components are comparable to the instrument profile FWHM and are, currently, very uncertain.

Table III provides values of $v_{1/e}$ for the broad components and the broad component fractions of the line intensity for detector rows (see Figure 15) corresponding to plume concentrations (rows 27−31 and 36−39), between plume concentrations (rows 23−27 and rows 32−35) and a region well outside plume concentrations (rows 5−17). The narrow components of both O VI lines are much stronger in the plume concentrations than in the other regions. These data suggest that polar plumes are the source regions of the narrow components observed at 1.7 $R_\odot$, and regions of the coronal hole outside the plumes are the source regions of the broad components for the observation of Figure 16. Stray light is expected to account for less than 5% of the narrow component of Figure 16(b). Observations from other time periods in 1996 are similar to Figure 16, but the enhancement of the narrow component is smaller. There is a tendency for the LOS velocity distribution in plume concentrations to be more narrow than in regions away from plume concentrations. The O VI 1032 image for 31 May 1996 makes it clear that streamers

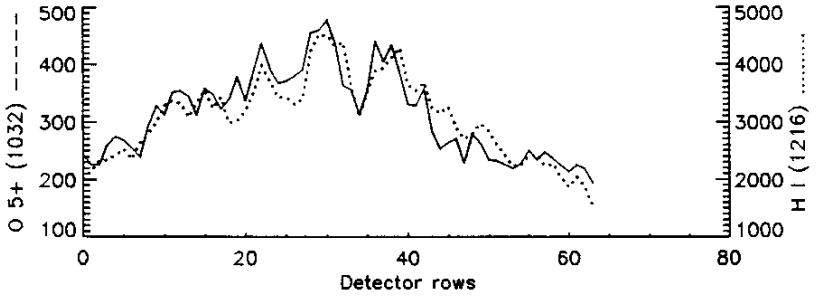

Figure 15. Variation of O VI 1032 Å (solid) and H I Lα (dots) intensities versus position along the instantaneous field of view, which corresponds to the UVCS/SOHO entrance slit, for an observation on 7 June 1996. The row numbers of the abscissa refer to spatial bins of 28 arc sec. The slit was oriented such that it was perpendicular to the radial line passing through the north solar pole and intersected it at 1.7 $R_\odot$ and row 30. The peaks in intensity apparently correspond to concentrations of polar plumes.

are outside the LOS for polar observations centered at 1.7 $R_\odot$ and so streamers are not the origin of the narrow O VI components for the observations of 7 June 1996. Observations at higher heights (see Figure 12) have much smaller narrow components that may be entirely due to stray disk light plus F corona.

Figure 14 is a plot of $v_{1/e}$ versus heliographic height for the north polar coronal hole as observed on 7 April 1996. It also includes data for the June 1996 observations. The data plotted are for single Gaussian coronal profiles which were obtained with the constrained curve fit procedure described earlier. Differences in the values for O VI 1032 and 1037 are believed to fall within the uncertainty limits. In general, the O^{5+} values of $v_{1/e}$ are smaller than those for H^0 at 1.5 $R_\odot$, comparable to H^0 at about 1.7 $R_\odot$ and significantly larger than those for H^0 at 2.1 $R_\odot$. The Mg X 625 Å line has $v_{1/e}$ between those of O^{5+} and H^0 at 1.5 $R_\odot$ and comparable or slightly larger values than both at 1.75 $R_\odot$.

It is interesting to compare the H^0 and O^{5+} values for $v_{1/e}$ at 2.1 $R_\odot$. The H^0 value of 200 km s^{-1} is considerably smaller than the O^{5+} value of 485 km s^{-1} for the June 1996 data. The O^{5+} values for 7 April 1996 are slightly smaller than those for June 1996, but still significantly larger than the H^0 value.

Recent calculations by Olsen and Leer (1996) and by Allen, Habbal, and Hu (1996) indicate that the H^0 velocities at 2.5 $R_\odot$ should be representative of the proton motions. Since transverse wave motion should be nearly the same for O^{5+} and protons, the observed velocities for H^0 and O^{5+} suggest that something other than transverse wave motion is contributing, significantly, to the O^{5+} velocity distribution. The explanation might be that the larger $v_{1/e}$ for O^{5+} is a result of ion-cyclotron resonant acceleration of O^{5+} ions about the coronal magnetic field lines (McKenzie, Banaszkiewicz, and Axford, 1995). More experimental and theoretical work is needed to resolve this issue.

Table III
UVCS/SOHO O VI 1032 and 1037 Å parameters for different concentrations of plumes

λ (Å)	Rows	I_B / I_{tot}	$v_{1/e}$ (km s^{-1})
1032	27–31 and 36–39	0.55	280
1037	36–39	0.47	370
1032	23–27 and 32–35	0.85	230
1037	32–35	0.719	290
1032	5–17	0.74	310
1037	5–17	0.86	330

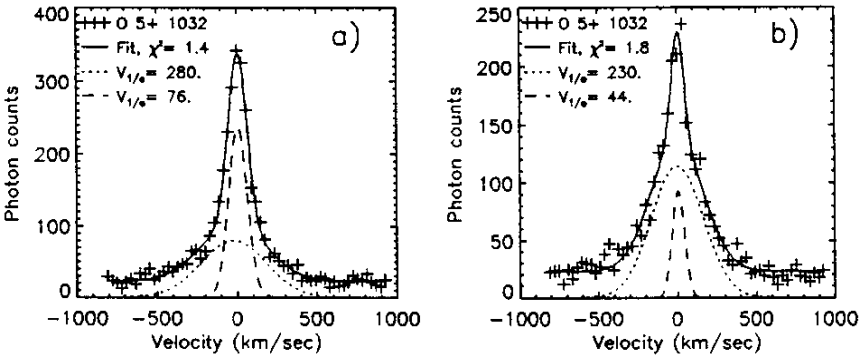

Figure 16. UVCS/SOHO 7 June 1996 observations of O VI 1032 Å profiles for regions in the brightest polar plume concentrations (a) and between plume concentrations (b). The observations are for the north polar coronal hole and combine rows 27–31 and 36–39 (a) and rows 23–27 and 32–35 (b) (see Figure 15). Row 30 corresponds to a heliocentric height of 1.7 $R_{\odot}$, the slit width corresponds to 8.7 arc sec, the FWHM of the instrument profile is 0.16 Å and the integration time is 16 000 s. The data points are shown by crosses, the fitted components by dots and dashes and the fitted profile by a solid line. The best fit $v_{1/e}$ and the $\nu^{-1}\chi^2_{\text{min}}$ are provided in the figure.

8. Preliminary Doppler Dimming Measurements in Helmet Streamers

The outflow velocity of O^{5+} in the equatorial streamer above the west limb of the Sun on 5 February 1997 can be estimated from the intensity ratio of O VI 1032 Å to O VI 1037 Å (see discussion in Section 3). Figure 17 is a plot of that ratio versus heliocentric height along a nearly straight line near the axis of the streamer. The 5 February 1997 streamer is similar in appearance to the one shown in Figure 6. Observations of the former include larger heights.

As discussed in Section 3, the resonantly scattered components have a ratio of 4:1 for velocities less than about 100 km s^{-1} and the collisional components have a ratio of 2:1 at all heights. Ratios above 2 indicate that the O^{5+} outflow velocity is less than about 100 km s^{-1} (see Figure 1) where we assume for the moment, that $v_{1/e}$ in the direction of the incoming radiation is less than 56 km s^{-1}. The

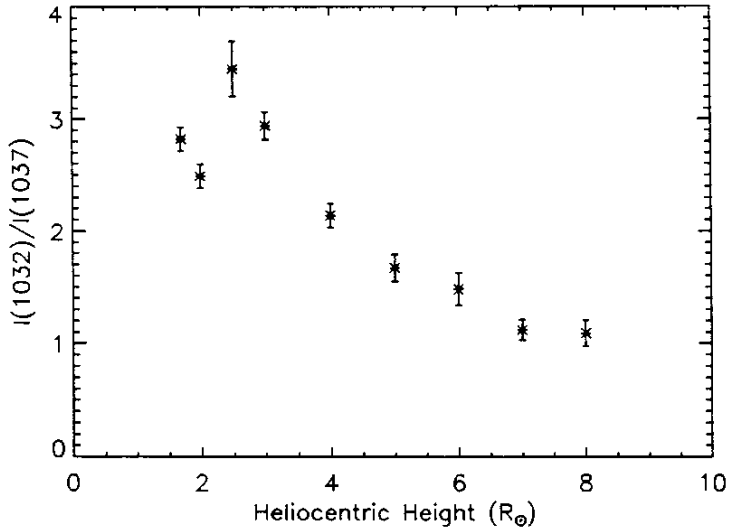

Figure 17. Observed intensity ratio for O VI 1032 Å to O VI 1037 Å near the axis of an equatorial streamer above the west solar limb on 5 February 1997. The error bars are for 1 standard deviation in the ratio.

plot of Figure 17 indicates that the ratio is above 2 for heights less than 4 $R_\odot$. The increase in the ratio from 1.7 $R_\odot$ to 2.5 $R_\odot$ is probably due (at least in part) to a decrease in electron density with height. UVCS/WLC measurements of polarized radiance, which is proportional to electron density, indicate that the electron density decreases with height in the streamer. The intensity of the collisional components scale as the square of the electron density and the resonantly scattered components scale linearly with electron density. The observed increase in the ratio from about 2.5 to 3.5 indicates that the O^{5+} outflow velocity remains below 100 km s^{-1} and the collisional component decreases with height as expected.

Since the collisional component will continue to decrease with height, the observed decrease in the ratio from about 3.5 to 2.0 between 2.5 $R_\odot$ and 4.0 $R_\odot$ indicates that Doppler dimming of the resonantly scattered components occurs at those heights since, otherwise, the resonant components would become more dominant.

At 4 $R_\odot$ the ratio becomes approximately 2. The Doppler dimming of both O VI lines is the same for velocities less than about 100 km s^{-1}. Hence, a ratio of 2 indicates that the resonantly scattered components of both lines are negligible. This occurs when the O^{5+} outflow velocity reaches about 100 km s^{-1}.

The observed decrease in the ratio below 2 indicates that the resonantly scattered component of the O VI 1037 line is larger than that of O VI 1032. This is expected to occur when the O^{5+} outflow velocity is large enough for the chromospheric C II 1037.018 Å radiation to be Doppler-shifted enough to overlap with the coronal

absorption line profile of O VI 1037.613 Å. The precise outflow velocity required to allow this pumping depends on the spectral width of the chromospheric emergent intensity and the width of the coronal absorption profile.

Figure 18 is a plot of the O VI line ratio versus O^{5+} outflow velocity for an electron density at 7 $R_\odot$ of 4.4 $\times$ 10^4 cm^{-3}. This value is derived from measurements of visible polarized radiance assuming a spherically-symmetric corona. This approach yields a lower limit for the electron density at 7 $R_\odot$ in the 5 February 1997 streamer. Curves for seven different coronal absorption line widths are provided. These line widths depend on the velocity distribution of the coronal O^{5+} in the direction of the incoming C II chromospheric radiation. In the figure, this velocity distribution is designated by the value of $v_{1/e}$ for the approximately radial direction. The curves of Figure 18 take into account both the collisional and resonantly scattered components of the two lines for the above density. Higher electron densities will raise the curves to higher line ratios for the same kinetic temperature. This occurs because the collisional components, which have a 2:1 ratio, will be relatively brighter for the higher densities. The O VI line ratio is not sensitive to the electron temperature or to the elemental abundance.

The line ratio at 7 $R_\odot$ is 1.1 which corresponds to 56 km s^{-1} for $v_{1/e}$ in the direction of the incoming radiation. This is an upper limit on $v_{1/e}$ for that direction since the electron density used here is a lower limit and higher electron densities raise the curves of Figure 18.

Although we do not have a measurement for $v_{1/e}$ of O^{5+} for the LOS direction in the streamer at 7 $R_\odot$, the upper limit derived above for the incoming radiation direction is significantly less than the LOS values for the highest heights provided in Figure 8.

The O^{5+} outflow velocity at 7 $R_\odot$ derived from Figure 18 is between 175 and 205 km s^{-1}. The discussion above about the O VI ratio at lower heights assumed the Doppler dimming curves of Figure 1 for the case where $v_{1/e}$ is less than 56 km s^{-1} for the velocity distribution in the incoming radiation direction. Hence, the O^{5+} outflow velocity values discussed earlier for the lower heights in the streamer are approximately correct.

It is important to recognize that the derived O^{5+} outflow velocity is not necessarily equal to that of the protons. Doppler dimming of H I Lα can be used to estimate the proton outflow velocity.

Although the approach outlined above provides a reasonably accurate estimate of the O^{5+} outflow velocities in the observed equatorial streamer, more precise values could be obtained with a self-consistent empirical model of the O VI intensity ratio and the absolute O VI intensities as well as an analysis of Doppler dimming in H I Lα. That model would require independent determinations of the electron temperature and electron density. It is also desirable to estimate the LOS contributions to the observed intensities. The UVCS synoptic data can be used for that purpose.

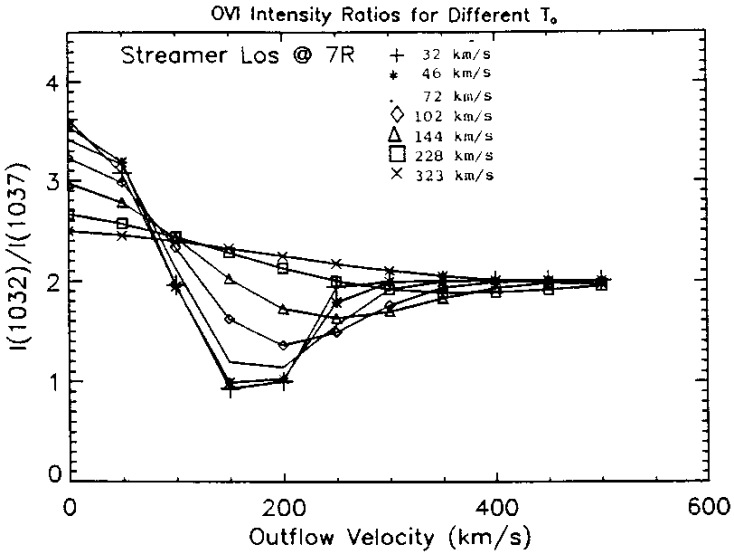

Figure 18. Modeled intensity ratio for O VI 1032 Å to O VI 1037 Å versus outflow velocity for a spherically-symmetric corona with an electron density that reproduces the observed visible polarized radiance at a heliocentric height of 7 $R_\odot$ for an equatorial streamer above the west solar limb on 5 February 1997. Seven curves are provided for different velocity distributions for the coronal O^{5+} in the direction of incoming C II radiation from the chromosphere. The curves are labled with the value of $v_{1/e}$ for the velocity distribution in the direction of the incoming radiation.

9. Preliminary Doppler Dimming Measurements in Polar Coronal Holes

Outflow velocities for O^{5+} can be estimated for polar coronal holes in the same manner used for the streamer in Section 8, Figure 19 is a plot of the O VI 1032/1037 ratio for the north polar coronal hole which was observed during the month of January 1997. The data used for the line ratios are standard UVCS synoptic observations for heliocentric heights between 1.5 and 2.5 $R_\odot$ and a series of special observations at 3 $R_\odot$. Stray light plus F corona and detector backgrounds have been removed from the data. The statistical error bars are vanishingly small on the plot.

The ratio is about 2.5 at 1.5 and 1.75 $R_\odot$. This ratio implies that the O VI 1032 line has a resonantly scattered component. If we assume that the Doppler dimming curve in Figure 1 (for $v_{1/e}$ less than 91 km s^{-1} in the direction of the incoming radiation) is applicable, then the O^{5+} outflow velocity is less than 150 km s^{-1}. However, if the velocity distribution in the direction of the incoming O VI transition region radiation is as wide as the observed line widths in the LOS direction (see Section 7), then the appropriate Doppler dimming curve would be much different.

The ratio reaches 2 at 2 $R_\odot$. If we again assume that Figure 1 is applicable, then the O^{5+} outflow velocity is expected to be between 100 km s^{-1} and 125 km s^{-1} for radial values of $v_{1/e}$ from 32 km s^{-1} to 91 km s^{-1}.

The ratio decreases from 2 to 0.7 over a range of heights from 2 to 3 $R_\odot$. The only known explanation for the ratio falling below two is pumping of O VI 1037.613 Å by the C II 1037.018 Å line.

Figure 20 is a plot of the O VI line ratio versus O^{5+} outflow velocity for a spherically-symmetric electron density with 6×10^4 cm^{-3} at 3 $R_\odot$. This model is consistent with observed visible polarized radiance values for 3 $R_\odot$ in the January 1997 polar coronal hole. Curves for seven different coronal absorption line widths are provided. These line widths depend on the velocity distribution of the coronal O^{5+} in the direction of the incoming C II chromospheric radiation. In the figure, this velocity distribution is designated by the value of $v_{1/e}$ for the approximately radial direction. The curves of Figure 20 take into account both the collisional and resonantly scattered components of the two lines for the above density. The ratio is not sensitive to the electron temperature or to the elemental abundance.

The line ratio at 3 $R_\odot$ is 0.70 which corresponds to $v_{1/e}$ less than 91 km s^{-1} in the direction of the incoming radiation.

The value for $v_{1/e}$ in the LOS direction for O^{5+} in the January coronal hole at 3 $R_\odot$ is about 600 km s^{-1}. The upper limit derived above for the $v_{1/e}$ in the direction of the incoming radiation is significantly less. Since the direction of the incoming radiation is approximately parallel to the expected magnetic field direction in polar coronal holes, and the LOS direction is approximately perpendicular to the field, it appears that $v_{1/e}$ parallel to the magnetic field is significantly smaller than $v_{1/e}$ in the perpendicular direction.

The O^{5+} outflow velocity at 3 $R_\odot$ derived from Figure 20 is between 130 and 230 km s^{-1}. The discussion above about the O VI ratio at lower heights referred to the Doppler dimming curves of Figure 1 where the value of $v_{1/e}$ in the direction of the incoming radiation was assumed to be less than 91 km s^{-1}. Hence, the discussion of the O^{5+} outflow velocities at lower heights should be reasonably accurate.

It is important to recognize that the derived O^{5+} outflow velocity is not necessarily equal to that of the protons. Doppler dimming of H I Lα can be used to estimate the proton velocity.

The estimates of outflow velocity from the above procedure treat the coronal hole as a section of a spherically-symmetric source. However, it is apparent from the observations that polar coronal holes contain polar plumes that extend up to several solar radii. It could be seen from Section 7 that the O VI spectral line widths in plumes at 1.7 $R_\odot$ appear to be much smaller than those away from plume concentrations. The density in plumes is believed to be considerably larger than in the interplume regions. The outflow velocity in plumes is unknown at the present time.

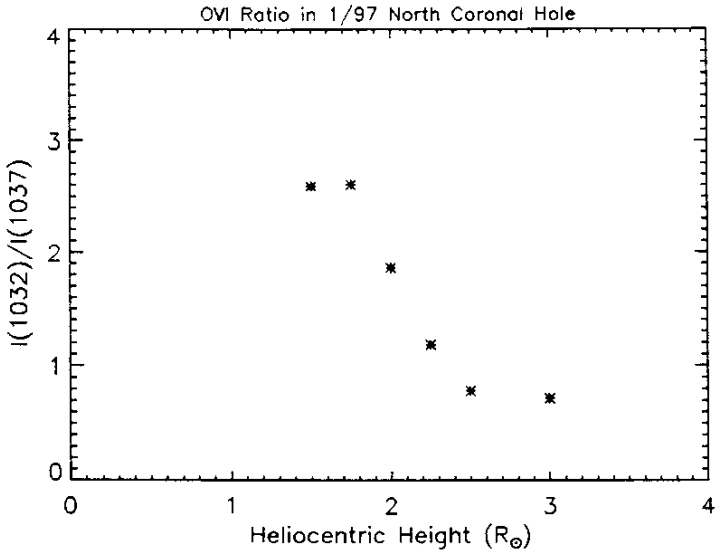

Figure 19. Observed intensity ratio for O VI 1032 Å to O VI 1037 Å near the axis of the north polar coronal hole as observed during the month of January 1997. The statistical error bars are too small to be disernible from the data points.

10. Summary

This paper provides examples of UVCS/SOHO spectroscopic observations of the extended solar corona during the first year of operations. Values are presented for velocity distributions of protons and minor ions and for O^{5+} outflow velocities in equatorial streamers and polar coronal holes. The results presented here are obtained from direct application of spectroscopic diagnostic techniques. More precise values can be obtained by developing a self-consistent empirical model that specifies densities, velocity distributions, and outflow velocities for the primary particles and several minor ions, and also specifies abundances relative to hydrogen. The models should specify local values for plasma parameters in three dimensions. For structures that are stable for a few days, daily UVCS synoptic observations, which began on 10 April 1996, can be used to help determine the three dimensional structure of the observed corona.

Measurements of spectral line profiles for H I Lα and Lβ, O VI 1032 Å and 1037 Å, S X 1196 Å, and Fe XII 1242 Å in equatorial streamers provide measurements of LOS values for the velocity distribution of the associated ions (specified by $v_{1/e}$). At heliocentric heights of 1.5 $R_\odot$ in equatorial streamers where the density is the highest, the $v_{1/e}$ along the LOS approach those of a thermal distribution at about 2×10^6 K. This value is in approximate agreement with the electron temperature derived from the ionization balance of hydrogen. Departures from thermal values

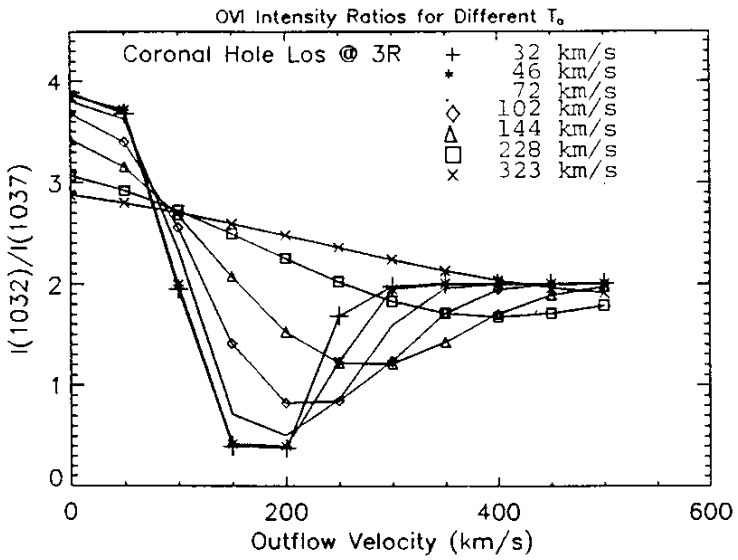

Figure 20. Modeled intensity ratio for O VI 1032 Å to O VI 1037 Å versus outflow velocity for a spherically-symmetric corona with an electron density that reproduces the observed visible polarized radiance at a heliocentric height of 3 $R_\odot$ for the north polar coronal hole observed during the month of January 1997. Seven curves are provided for different velocity distributions for the coronal O^{5+} in the direction of incoming C II radiation from the chromosphere. The curves are labled with a value of $v_{1/e}$ for the velocity distribution in the direction of the incoming radiation.

become larger with increasing mass. The $v_{1/e}$ for H^0 decrease from a maximum value of about 180 km s^{-1} at about 2 $R_\odot$ to about 140 km s^{-1} at 8 $R_\odot$. The $v_{1/e}$ for O^{5+} increase with height and reach values of 150 km s^{-1} at 4.7 solar radii which are approximately equal to the H^0 values. The observed velocities come closest to a thermal distribution in the highest density regions of equatorial streamers. In lower density structures, the $v_{1/e}$ show larger departures from equilibrium values with increasing mass. It appears that some process is preferentially accelerating particles of higher mass, and collisions are driving the velocities toward thermal equilibrium.

Measurements of the intensity ratio of O VI 1032 Å and 1037 Å have been used to estimate outflow velocities of O^{5+} ions in equatorial streamers. The O^{5+} outflow velocity is found to be less than 100 km s^{-1} below 3.5 $R_\odot$ and reaches a value of about 100 km s^{-1} at 4 $R_\odot$. The outflow velocity reaches a value of 175 to 205 km s^{-1} at 7 $R_\odot$.

The O VI line ratio was also used to estimate the $v_{1/e}$ for O^{5+} in the direction of the incoming radiation from the chromosphere. It is found that the $v_{1/e}$ in that direction at 7 $R_\odot$ in the observed equatorial streamer is less than 56 km s^{-1}. The

O^{5+} values of $v_{1/e}$ for the LOS direction at 7 $R_\odot$ have not been measured but the value at 5 solar radii is 150 km s^{-1}.

UVCS observations of coronal holes at 1.7 $R_\odot$ in H I Lα, O VI 1032 Å and O VI 1037 Å indicate bright ray-like structures that are likely to be concentrations of polar plumes along the LOS.

Both UVCS/SOHO and Spartan 201 observations indicate that a significant fraction of the protons along the LOS in coronal holes have $v_{1/e}$ larger than expected for a Maxwellian velocity distribution at the expected electron temperature of about 1×10^6 K. UVCS/SOHO observations, after removal of stray light plus F corona and interplanetary Lα, yield good constrained curve fits to single Gaussians for the coronal line profiles of H I Lα and O VI 1032 and 1037 at heights above 2.0 $R_\odot$.

If one compares the $v_{1/e}$ of O^{5+} and H^0 for various heights in polar coronal holes, one finds that the O^{5+} $v_{1/e}$ are smaller than those of H^0 at 1.5 $R_\odot$, are comparable at about 1.7 $R_\odot$ and become significantly larger than those of H^0 at 2.1 $R_\odot$. Mg^{9+} $v_{1/e}$ are larger than those of both H^0 and O^{5+} at 1.7 $R_\odot$.

Measurements of the intensity ratio of O VI 1032 Å and 1037 Å have been used to estimate outflow velocities of O^{5+} ions in polar coronal holes. The O^{5+} outflow velocity is found to be less than 150 km s^{-1} below 1.7 $R_\odot$ and reaches a value between 100 km s^{-1} and 125 km s^{-1} at 2 $R_\odot$. The outflow velocity reaches a value between 130 and 230 km s^{-1} at 3 $R_\odot$.

The O VI line ratio was also used to estimate the $v_{1/e}$ in the direction of the incoming radiation to coronal O^{5+} from the chromosphere. It is found that the $v_{1/e}$ in that direction at 3 $R_\odot$ in the observed polar coronal hole is less than 91 km s^{-1}. The O^{5+} values of $v_{1/e}$ for the LOS direction at 3 $R_\odot$ have been determined to be about 600 km s^{-1}. Since the direction of the incoming radiation is approximately parallel to the expected magnetic field direction in polar coronal holes, and the LOS direction is approximately perpendicular to the field direction, it appears that $v_{1/e}$ parallel to the magnetic field is significantly smaller than $v_{1/e}$ in the perpendicular direction.

The differences of the $v_{1/e}$ with mass in coronal holes suggests that very significant fractions of the O^{5+} velocities are not caused directly by transverse wave motions. The outflow velocities are expected to be too small to contribute significantly to the $v_{1/e}$. It appears that some microscopic motion (perhaps ion-cyclotron resonant acceleration) is the dominant process responsible for the observed difference between the $v_{1/e}$ for O^{5+} and H^0.

There is a tendency for the O^{5+} LOS velocity distribution in plume concentrations to be more narrow than the distribution in regions away from plume concentrations.

There are several types of observations that are not reported in this paper, but are in process. They include direct measurements of electron temperatures derived from measurements of the spectral line profile of coronal electron scattered H I Lα from the chromosphere, and determinations of proton outflow velocities

derived from measurements of visible polarized radiance and Doppler dimming of resonantly scattered H I Lα. UVCS determinations of minor ion abundances in streamers are presented elsewhere in this volume (Raymond *et al.*, 1997). UVCS has observed several CMEs in the extended corona where the intensities of the H I Lyman series and ions at low stages of ionization are enhanced by two to three orders of magnitude over their usual values. There have also been observations of a comet in H I Lα, observations of several stars at wavelengths shortward of the Hubble Space Telescope range and observations of interplanetary H I 1216 Å and He I 584 Å.

UVCS/SOHO has also made many coordinated observations with other instruments on SOHO, with instruments on other satellites and with ground-based observatories. Among the most important of those are coordinated observations with SOHO's CELIAS, LASCO, SUMER, SWAN, MDI, and CDS. Coordinated observations of particular interest also include solar wind properties with *Ulysses*, CMEs with *Yohkoh*, and measurements of solar wind velocities and properties with radio scintillation measurements through the corona from astronomical sources and man-made satellites.

Acknowledgements

The authors wish to acknowledge the contributions of A. van Ballegooijen to the development of the UVCS instrument and the work of Brenda Bernard in the administration of the UVCS investigation. This work is supported by the National Aeronautics and Space Administration under grant NAG5−3192 to the Smithsonian Astrophysical Observatory, by Agenzia Spaziale Italiana and by Swiss funding through ESA's PRODEX programs, national funds and the Swiss Federal Institute of Technology Zürich.

References

Allen, L. A., Habbal, S. R., and Hu, Y. Q.: 1996, *J. Geophys. Res*, submitted.

Bevington, P. R.: 1969, *Data Reduction and Error Analysis for the Physical Sciences*, McGraw-Hill Book Co., New York, p. 313.

Gardner, L. D., Kohl, J. L., Daigneau, P. S., Dennis, E. F., Fineschi, S., Michels, J., Nystrom, G. U., Panasyuk, A., Raymond, J. C., Reisenfeld, D.= J., Smith, P. I,., Strachan, L., Jr., Suleiman, R., Noci, G. G., Romoli, M., Ciaravella, A., Modigliani, A., Huber, M. C. E., Antonucci, E., Benna, C., Giordano, S., Tondello, G., Nicolosi, P., Naletto, G., Pernechele, C., Spadaro, D., Siegmund, O. H. W., Allegra, A., Carosso, P. A., and Jhabvala, M. D.: 1996, 'Stray Light, Radiometric, and Spectral Characterization of UVCS/SOHO: in R. E. Huffman and C. G. Stergis (eds), Laboratory Calibration and Flight Performance', *Ultraviolet Atmospheric and Space Remote Sensing: Methods and Instrumentation*, SPIE 2831, p. 2.

Gouttebroze, P., Lemaire, P., Vial, J. C., and Artzner, G.: 1978, *Astrophys. J.* **225**, 655.

Ko, Y., Fisk, L. A., Geiss, J., Gloeckler, G., and Guhathakurta, M.: 1997, *Solar Phys.* **171**, 345.

Kohl, J. L. and Withbroe, G. L.: 1982, *Astrophys. J.* **256**, 263.

Kohl, J. L., Strachan, L., and Gardner, L. D.: 1996, *Astrophys. J.* **465**, L141.

Kohl, J. L., Esser, R., Gardner, L. D., Habbal, S., Daigneau, P. S., Dennis, E. F., Nystrom, G. U., Panasyuk, A., Raymond, J. C., Smith, P. L., Strachan, L., van Ballegooijen, A. A., Noci, G., Fineschi, S., Romoli, M., Ciaravella, A., Modigliani, A., Huber, M. C. E., Antonucci, E., Benna, C., Giordano, S., Tondello, G., Nicolosi, P., Naletto, G., Pernechele, C., Spadaro, D., Poletto, G., Livi, S., von der Luhe, O., Geiss, J., Timothy, J. G., Gloeckler, G., Allegra, A., Basile, G., Brusa, R., Wood, B., Siegmund, O. H. W., Fowler, W., Fisher, R., and Jhabvala, M.: 1995, *Solar Phys.* **162**, 313.

McKenzie, J. F., Banaszkiewicz, M., and Axford, W. I.: 1995, *Astron. Astrophys.* **303**, L45.

Leer, E.: 1988, 'Solar Wind Conference' in V. J. Pizzo, T. E. Holzer, and D. G. Sime (eds), *Proc. 6th Int. Solar Wind Conference*, Boulder, CO, p. 89.

Noci, G., Kohl, J. L., and Withbroe, G. L.: 1987, *Astrophys. J.* **315**, 706.

Noci, G., Kohl, J. L., Antonucci, E., Tondello, G., Huber, M. C. E., Fineschi, S., Gardner, L. D., Naletto, G., Nicolosi, P., Raymond, J. C., Romoli, M., Spadaro, D., van Ballegooijen, A. A., Siegmund, O. H. W., Benna, C., Ciaravella, A., Giordano, S., Michels, J., Modigliani, A., Panasyuk, A., Pernechele, C., Poletto, G., Smith, P. L., and Strachan, L.: 1997, *Advances in Space Research, Cospar Proceedings*, in press.

Olsen, E. L. and Leer, E.: 1996, *Astrophys. J.* **462**, 982.

Pernechele, C., Naletto, G., Nicolosi, P., Poletto, L., and Tondello, G.: 1995, *Proc. SPIE* **2517**.

Raymond, J. C., Kohl, J. L., Noci, G., Antonucci, E., Tondello, G., Huber, M. C. E., Gardner, L. D., Nicolosi, P., Fineschi, S., Romoli, M., Spadaro, D., Siegmund, O. H. W., Benna, C., Ciaravella, A., Cranmer, S., Giordano, S., Karovska, M., Martin, R., Michels, J., Modigliani, A., Naletto, M. G., Panasyuk, A., Pernechele, C., Poletto, G., Smith, P. L., Suleiman, R. M., and Strachan, L.: 1997, *Solar Phys.*, in press.

Strachan, L., Kohl, J. L., Weiser, H., and Withbroe, G. L.: 1993, *Astrophys. J.* **412**, 410.

Strachan, L., Gardner, I. D., Hassler, D. M., and Kohl, J. L.: 1994, *Space Sci. Rev.* **70**, 263.

van de Hulst, H. C.: 1950, *Bull. Astron. Inst. Neth.* **11**, 135.

Wilhelm, K.: 1996, personal communication.

Withbroe, G. L., Kohl, J. L., Weiser, H., and Munro, R. H.: 1982, *Space Sci. Rev.* **33**, 17.

Withbroe, G. L., Kohl, J. L., Weiser, H., and Munro, R. H.: 1985, *Astrophys. J.* **297**, 324.